International Journal of Chemical Sciences

Research | Vol 16 Iss 1

FTIR, FT-Raman, SERS and Computational Studies of the Vibrational Spectra, Molecular Geometries and other Properties of 4-Fluoroaniline

Viswanathan K[1*], Jeyavijayan S[1], Praseeda K[2] and Gurushankar K[1]

[1]Department of Physics, Kalasalingam University, Anand Nagar, Krishnankoil 626 126, Tamil Nadu, India

[2]VHM Higher Secondary School, Morayur, Malappuram District, Kerala, India

[*]**Corresponding author:** Viswanathan K, Department of Physics, Kalasalingam University, Anand Nagar, Krishnankoil 626 126, Tamil Nadu, India, Tel: +91-9443367493; E-mail: viswanathan.k@klu.ac.in

Received: December 12, 2017; **Accepted:** January 17, 2018; **Published:** January 20, 2018

Abstract

The FTIR (4000 cm^{-1}-450 cm^{-1}), FT-Raman and SERS (4000 cm^{-1}-50 cm^{-1}) spectra of 4-fluoroaniline (4FA) have been recorded. The DFT/B3LYP method is used to compute the vibrational frequencies. Tentative assignments of the observed and computed wavenumbers are provided. The observed and scaled wavenumber values show very good agreement. Optimized geometrical parameters and frontier molecular orbitals are carried out by DFT/B3LYP method combined with 6-31+G (d, p) and 6-311++G (d, p) basis sets. Further, the molecular electrostatic potential (MEP) and the first order hyperpolarizability are investigated using theoretical calculations. In addition, the Mulliken's charges analysis and several thermodynamic properties were calculated.

Keywords: FTIR; FT-Raman; SERS; 4-fluoroaniline; DFT calculations

Citation: Viswanathan K, Jeyavijayan S, Praseeda K, et al. FTIR, FT-Raman, SERS and Computational Studies of the Vibrational Spectra, Molecular Geometries and other Properties of 4-Fluoroaniline. Int J Chem Sci. 2018;16(1):241

Introduction

In the synthesis of a large amount of dyes, pharmaceuticals, chemicals and electro-optical industrial processes, aniline and its derivatives are used widely used as starting materials [1]. Polyaniline, the conducting polymer of aniline, is used as diodes and transistors in microelectronic devices. Derivatives of aniline are used particularly in the production of pesticides, antioxidants and dyes [2,3]. Wojciechowski et al. have investigated para-halogen anilines and the theoretical infrared and Raman spectra and vibrational assignments are done [4]. Kavitha et al. [5] have studied the vibrational spectra, molecular structure and HOMO, LUMO studies of 4-nitroaniline. Arjunan et al. [6] have reported the studies of vibrational spectra and non-linear optical properties of 2-(trifluoromethyl) aniline and 3-(trifluoromethyl) aniline. Moreover, Femina Jasmine et al. [7] have reported the molecular structure and charge transfer contributions to nonlinear optical property of 2-methyl-4-nitroaniline. More recently, Revathi et al. [8] deliberated the NLO properties of 4-chloro-3-(trifluoromethyl) aniline, 4-bromo-3-(trifluoromethyl) aniline and 4-fluoro-3-(trifluoromethyl) aniline. However, no density functional theory (DFT) with 6-31+G (d, p) and 6-311++G (d, p) basis set calculations of 4-fluoro aniline (4FA) have been reported so far, to the best of our knowledge. Therefore, in the present work an attempt has been made to study the detailed theoretical and experimental investigation of the vibrational spectra of 4FA.

Experimental

The fine polycrystalline sample of 4FA was obtained from Lancaster Chemical Company, UK and used as such for spectral measurements. A Perkin Elmer Spectrum-1 FTIR Spectrometer, with a resolution of 1 cm^{-1}, was used to record the FTIR spectrum of the compound at room temperature, in the range 450 cm^{-1} to 4000 cm^{-1}. The sample was taken in a cuvette.

The sample solution was prepared in three different concentrations using de-ionized water, with sample to water ratios 1:5 (S1), 1:10 (S2) and 1:20 (S3). The Raman spectra were recorded for three samples S1, S2 and S3, using BRUKER RFS 27, a multi-RAM stand-alone model, Raman spectrophotometer, in the spectral range is 4000 cm^{-1}-50 cm^{-1}, using the 1064 nm line of Nd:YAG laser, operating at 200 mW power. The reported wavenumbers are believed to be accurate within ± 1 cm^{-1}. The SERS spectra were recorded using the same Raman spectrophotometer, by mixing the samples with silver sol prepared by Crieghton method [9], at two sample-sol ratios (1:5 and 1:10).

Computational details

The observed bands of the molecule are to be essentially assigned to the different vibrations, for solving various chemical and structural problems. To understand the Raman and IR bands well, these have to be essentially assigned to different vibrations of the molecule. The industrial importance of substituted anilines prompted the authors to undertake an extensive spectroscopic study of 4FA. The FTIR, FT-Raman and SERS spectra at different concentrations are recorded for the compound and an effort has been made to give possible explanation for the vibrational fundamentals and to understand the effect of halogen group substitution on the characteristic frequencies of the amino group. The software package GAUSSIAN 09W [10] at the DFT/B3LYP level, combined with 6-31+G (d, p) and 6-311++G (d, p) basis sets, has been used to estimate the optimized structural parameters, optimized minimum energy, vibrational frequencies, IR intensity and Raman activity, for the

compound. In order to improve the agreement of theoretically calculated frequencies with experimentally calculated frequencies, it is essential to scale down the theoretically calculated harmonic frequencies. Hence, MOLVIB 7.0 version written by Tom Sundius [11,12], was used to scale down the theoretically calculated vibrational frequencies.

Results and Discussion

Molecular geometry

FIG. 1 shows the molecular structure (optimized) of 4FA having C_1 point group symmetry. The global minimum energy obtained by the DFT structure optimization with 6-31+G (d, p) and 6-31+G (d, p) basis sets for 4FA is calculated as -386.86972381 Hartrees and -386.95473148 Hartrees. TABLE 1 shows the optimized geometrical parameters for 4FA obtained by B3LYP method with 6-31+G (d, p) and 6-311++G (d, p) basis set calculations. It can be seen that the bond lengths estimated in both the sets are almost equal.

The geometrical parameters, estimated theoretically, give a good approximation and these are used as bases for calculating the vibrational frequencies, thermodynamics properties etc. It can be seen that the benzene ring is slightly distorted and angles are out of perfect hexagonal structure, slightly. The substitutions of the NH_2 group and fluorine atom in the place of H atoms, is responsible for this. As per the experimentally obtained values [13], order of the optimized length of the six C–C bonds of the ring are as C3–C4<C4–C5<C1–C2=C6–C1<C2–C3=C5–C6. According to the calculated values (B3LYP/6-311++G (d, p)), the order of the bond lengths is slightly differed as C3–C4=C4–C5<C2–C3=C5–C6<C1–C2=C6–C1, since the substitutions are different.

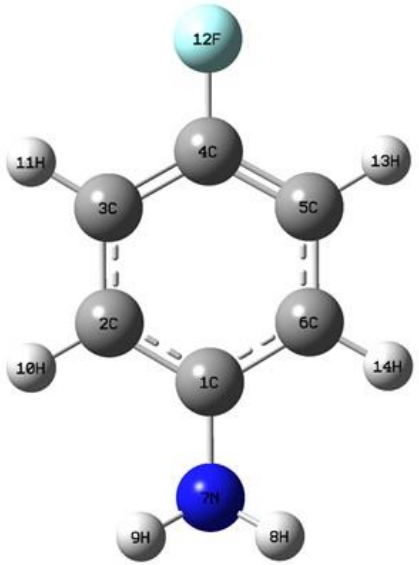

FIG. 1. **Molecular structure of 4-fluoroaniline.**

TABLE 1. **Optimized geometrical parameters for 4-fluoroaniline computed at B3LYP/6-31+G (d, p) and 6-311++G (d, p) basis sets.**

Bond length	Value (Å)		Expt[a]	Bond angle	Value (°)		Expt[a]
	B3LYP/ 6-31+G (d, p)	B3LYP/ 6-311++G (d, p)			B3LYP/ 6-31+G (d, p)	B3LYP/ 6-311++G (d, p)	
C_1–C_2	1.4058	1.4023	1.381	C_1–C_2 –C_3	120.9082	120.911	119.1
C_2–C_3	1.3958	1.3921	1.390	C_2–C_3–C_4	118.9604	119.056	118.5
C_3–C_4	1.3884	1.3849	1.372	C_3–C_4–C_5	121.7261	121.5828	123.2
C_4–C_5	1.3884	1.3849	1.373	C_4 –C_5–C_6	118.9593	119.0561	118.2
C_5–C_6	1.3958	1.3921	1.390	C_5–C_6–C_1	120.9091	120.911	119.2
C_6–C_1	1.4058	1.4023	1.381	C_6–C_1–C_2	118.5368	118.4829	121.8
C_1–N_7	1.4017	1.4008	1.464	C_6–C_1–N_7	120.695	120.7233	119.0
N_7–H_8	1.011	1.0095	0.93	C_2–C_1–N_7	120.6993	120.7232	119.3
N_7–H_9	1.011	1.0095	0.93	H_8–N_7–H_9	111.8115	111.7073	110.0
C_2–H_{10}	1.0869	1.085	0.95	C_1–C_2–H_{10}	119.6819	119.6746	120.0
C_3–H_{11}	1.0848	1.083	0.95	C_3–C_2–H_{10}	119.409	119.4136	121.0
C_4–F_{12}	1.3655	1.3614	1.363	C_2–C_3–H_{11}	121.1387	121.112	123.0
C_5–H_{13}	1.0848	1.083	0.97	C_4–C_3 –H_{11}	119.9009	119.832	118.0
C_6–H_{14}	1.0869	1.085	0.96	C_3–C_4–F_{12}	119.136	119.2086	118.2
-	-	-	-	C_5–C_4–F_{12}	119.1378	119.2086	118.6
-	-	-	-	C_4–C_5–H_{13}	119.9018	119.8319	121.0
-	-	-	-	C_6–C_5–H_{13}	121.1389	121.112	121.0
-	-	-	-	C_5–C_6–H_{14}	119.4127	119.4135	119.0
-	-	-	-	C_1–C_6–H_{14}	119.6771	119.6747	121.0
-	-	-	-	C_1–N_7–H_9	115.4728	115.3365	113.0
-	-	-	-	C_1–N_7–H_8	115.4825	115.3364	113.0

[a]Experimental values are taken from Ref. [13]

As seen from the TABLE 1, the bond length of C-N is found to be 1.4017 Å by B3LYP/6-31+G (d, p) method and is higher than other bond lengths, since nitrogen is electronegative in nature. For the title compound, the C-C bond lengths are in between 1.3884 and 1.4058 Å by DFT/B3LYP/6-31+G (d, p) method. In particular, the bond lengths of C1-C2 and C6-C1 are increased slightly with other bond lengths in the skeleton. The bond lengths of C-H appear in the characteristics region. The C–

F bond length indicates a considerable increase when substituted in place of C–H. Fluorine atom is in the plane of the benzene ring. The C–F bond length is found to be 1.363Å by expt. [13], 0.0016Å larger than the calculated value (1.3614Å) by B3LYP/6-311++G (d, p). Asymmetry of the benzene ring is also evident from the positive deviation of C3-C4-C5 and negative deviation of C6-C1-C2 bond-angles from the normal value of 120°, since the substitution of fluorine atom and NH_2 group at C4 and C1 atoms, respectively. Other C–C–C angles are calculated bigger and smaller than the hexagonal angle due to the effect of substitutions in the benzene ring.

Vibrational spectra

There are 14 atoms and its 36 normal modes of vibration, for the title compound, which are active both in IR and Raman spectra. TABLE 2 gives the detailed assignment of the vibrational bands of 4FA calculated by the DFT, with 6-31+G (d, p) and 6-311++G (d, p) basis sets, along with the theoretically estimated Raman and IR intensities and normal mode descriptions (characterized by TED). The FTIR spectrum of the sample is given in FIG. 2. The FIG. 3 shows the UV absorption spectrum of the silver sol. The peak observed at 390 nm shows the presence of silver nano particles in the colloid. The experimental FT-Raman spectra of the three solutions S1, S2 and S3 are shown in FIG. 4.

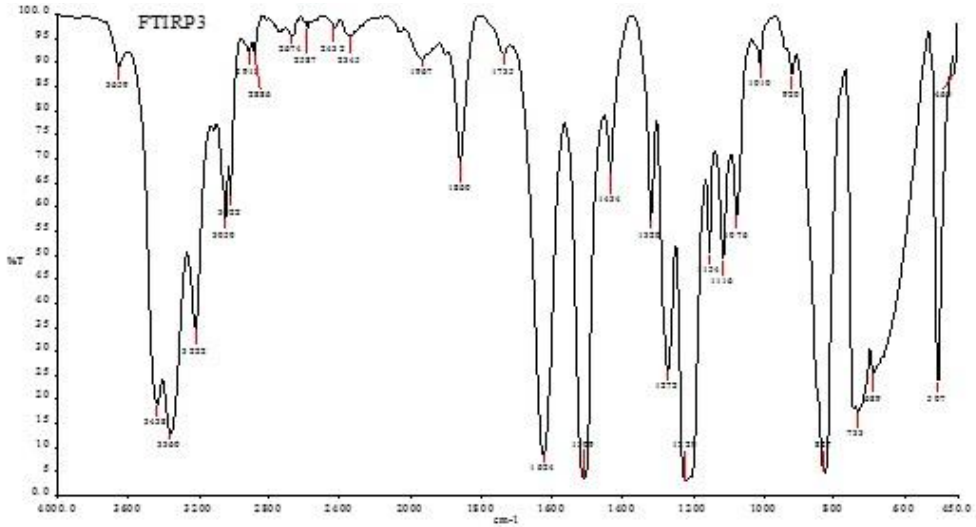

FIG. 2. **FTIR spectrum of 4-fluoroaniline.**

TABLE 2. **Vibrational assignments of fundamental modes of 4-fluoroaniline along with calculated IR intensity (km/mol), Raman activity (Å amu^{-1}) and normal mode descriptions (characterized by TED) based on quantum mechanical calculations using DFT method.**

Sl. No.	Species C_1	Observed fundamentals (cm^{-1})		Calculated frequencies ν_i (cm^{-1})								TED (%) among types of internal coordinates
				B3LYP/6-31+G(d,p)				B3LYP/6-311++G(d,p)				
		FTIR	Raman	Unscaled ν_i	Scaled	IR intensity[a]	Raman activity[b]	Unscaled ν_i	Scaled	IR intensity[a]	Raman activity[b]	
1	A	3659 (ms)	3506 (w)	3679	3535	17.01	53.22	3679	3535	16.22	57.16	NH_2 ass (99)
2	A	3438 (vs)	3424 (w)	3574	3434	16.99	173.52	3573	3433	15.75	189.61	NH_2 ss (98)
3	A	3360 (ms)	3360 (ms)	3217	3091	2.09	229.26	3216	3090	2.07	229.93	ν CH (96)
4	A	3222 (s)	3236 (ms)	3216	3090	4.20	51.59	3215	3089	4.25	51.68	ν CH (94)
5	A	3050 (ms)	3099 (w)	3181	3056	17.20	78.90	3181	3056	17.22	77.93	ν CH (92)
6	A	3022 (w)	3028 (vw)	3181	3056	11.24	81.69	3180	3055	11.32	82.27	ν CH (90)
7	A	1735 (vw)	-	1673	1607	68.67	27.33	1672	1606	67.82	28.96	ν CC (88)
8	A	1624 (vs)	-	1657	1592	19.69	4.58	1656	1591	20.07	4.14	NH_2 sciss (85)
9	A	-	1630 (w)	1645	1580	0.15	2.99	1645	1580	0.16	2.88	ν CC (84)
10	A	1509 (vs)	1530 (vw)	1548	1487	237.76	0.46	1548	1487	237.66	0.53	ν CC (86)
11	A	1434 (ms)	1458 (w)	1471	1413	0.27	0.36	1470	1412	0.27	0.38	ν CC (82)
12	A	-	1317 (w)	1361	1308	7.67	1.41	1361	1307	7.61	1.46	ν CC (80)
13	A	1320 (s)	-	1324	1272	0.01	2.17	1325	1273	0.01	2.21	ν CC (81)
14	A	1272 (s)	-	1302	1251	27.50	23.54	1302	1251	28.16	23.13	ν CN (78)
15	A	1220 (vs)	-	1239	1190	151.96	7.58	1239	1190	151.81	8.13	ν CF (76)
16	A	1154 (s)	-	1178	1132	3.49	8.12	1178	1132	3.48	8.13	b CH (75)
17	A	1116 (s)	-	1141	1096	11.15	0.02	1141	1096	11.29	0.03	b CH (74)
18	A	1076 (ms)	-	1079	1037	3.22	1.85	1079	1036	3.12	1.97	NH_2 rock (73)
19	A	1010 (w)	-	1025	985	2.27	0.02	1025	985	2.20	0.03	b CH (72)
20	A	-	949 (ms)	946	909	0.01	0.01	945	908	0.01	0.01	b CH (71)
21	A	920 (w)	930 (w)	930	893	1.25	0.05	927	891	1.67	0.31	ω CH (64)
22	A	-	856 (ms)	860	826	6.58	46.25	860	826	6.38	46.55	ω CH (65)
23	A	827 (vs)	-	835	802	81.74	0.82	834	801	81.45	0.97	ω CH (63)
24	A	-	802 (w)	807	775	0.03	0.54	807	775	0.03	0.25	ω CH (64)
25	A	733 (vw)	-	758	728	25.37	0.08	758	728	25.42	0.09	R asymd (70)
26	A	689 (w)	-	698	671	2.22	1.64	694	666	2.23	2.23	R trigd (69)
27	A	-	650 (w)	652	626	0.04	6.33	652	626	0.04	6.23	b CF (71)
28	A	-	555 (vw)	580	557	279.88	3.01	580	557	280.40	2.55	NH_2 wag (64)
29	A	507 (s)	-	508	488	70.47	0.58	508	488	70.01	0.67	R symd (68)
30	A	460 (vw)	-	462	444	2.29	8.12	462	443	2.30	8.10	t R trigd (65)
31	A	-	420 (vw)	436	419	1.72	0.32	436	419	1.72	0.31	t R symd (64)
32	A	-	397 (s)	426	409	0.35	0.01	426	409	0.35	0.03	t R asymd (65)
33	A	-	330 (vw)	358	344	7.89	3.36	357	343	7.71	2.81	b CF (67)
34	A	-	309 (ms)	330	317	0.14	0.43	330	317	0.13	0.43	ω CN (64)
35	A	-	250 (w)	254	244	19.81	0.21	251	241	19.81	0.24	ω CF (63)
36	A	-	150 (ms)	152	146	1.25	0.43	151	145	1.23	0.45	NH_2 twist (62)

Abbreviations used: ν-Stretching; ss: Symmetric Stretching; ass: Asymmetric Stretching; b: Bending; ω: Out-of-Plane Bending; R: Ring; t: Torsion; s: Strong; vs: Very Strong; ms: Medium Strong; w: Weak; vw: Very Weak

[a]Relative Absorption Intensities in km mol^{-1} and Normalized with the Highest Peak Absorbance

[b] Relative Raman Intensities in $Å^4amu^{-1}$ and normalized to 100

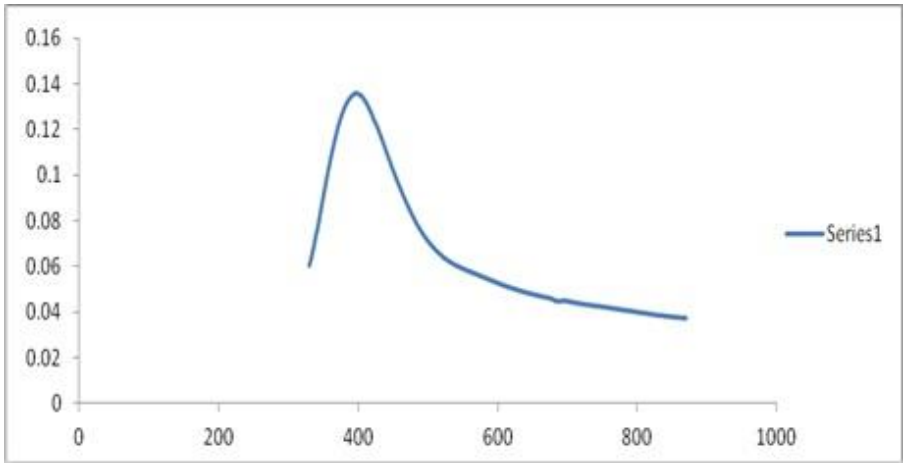

FIG. 3. **UV absorption spectrum of the silver sol.**

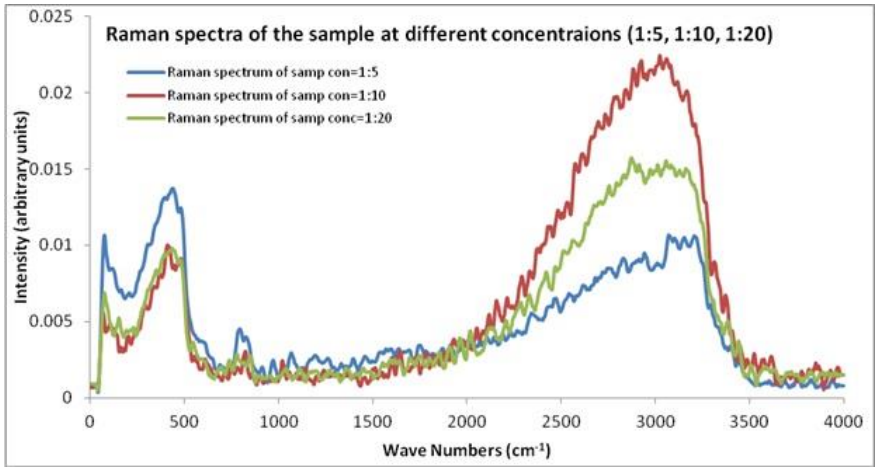

FIG. 4. **Raman spectra of the sample solutions (S1, S2, S3).**

Vibrational band assignments

The vibrational analysis involves the assignment of the bands observed at specific wave numbers in the IR and Raman spectra to the different vibrational modes giving rise to each of these observed bands.

C–H Vibrations

The C-H stretching vibrations of aromatic and hetero-aromatic structure are normally appearing in the region 3000-3100 cm^{-1} [14]. In this region, the bands are not affected appreciably by the nature of the substituent. Hence, in the present investigation, the C–H stretching vibrations of 4FA are observed at 3360 cm^{-1}, 3222 cm^{-1}, 3050 cm^{-1}, 3022 cm^{-1} in IR and 3360 cm^{-1}, 3236 cm^{-1}, 3099 cm^{-1}, 3028 cm^{-1} in Raman spectrum. Generally, the bands due to C-H in-plane bending vibrations interact with ring vibrations, are observed as a number of sharp bands in the region 1300 cm^{-1}-1000 cm^{-1}. The FTIR bands observed at 1154 cm^{-1}, 1116 cm^{-1}, 1010 cm^{-1} and Raman band found at 949 cm^{-1} are assigned to C–H in-plane bending vibrations of 4FA and these modes are confirmed by their TED values. The C–H out-of-plane bending vibrations of 4FA have also been identified and listed in TABLE 2.

C–C Vibrations

The bands between 1400 cm^{-1} and 1650 cm^{-1} in benzene derivatives are due to C–C stretching vibrations [15]. Therefore, the stretching vibrations of 4FA are observed at 1735 cm^{-1}, 1509 cm^{-1}, 1434 cm^{-1}, 1320 cm^{-1} in IR and 1630 cm^{-1}, 1530 cm^{-1}, 1458 cm^{-1}, 1317 cm^{-1} in Raman spectrum. The substitutions in the aromatic ring have affected most of the ring vibrational modes of the title compound. The bands observed in the FTIR spectra at 733 cm^{-1}, 689 cm^{-1} and 507 cm^{-1} have been assigned to ring in-plane bending modes. These modes are confirmed by their TED values. The ring out-of-plane bending modes of 4FA are also listed in the TABLE 2. Due to the change in force constant and the vibrations of the functional groups, the ring out-of-plane bending frequencies are reduced.

C–F Vibrations

In the vibrational spectra of related compounds, the bands due to C–F stretching vibrations [16] may be found over a wide frequency range 1360 cm^{-1}-1000 cm^{-1}, since the vibration is easily affected by adjacent atoms or groups. In the present investigation, the FTIR band observed at 1220 cm^{-1} has been assigned to C–F stretching mode of vibration for 4FA. The Raman bands found at 650 cm^{-1} and 250 cm^{-1} have been designated to C–F in-plane bending and out-of-plane bending modes, respectively.

C–N Vibrations

In aromatic compounds, the C–N stretching vibration usually lies in the region 1400 cm^{-1}-1200 cm^{-1}. The identification of C–N stretching frequencies is not an easy task, due to the possible mixing of vibrations in this region [17]. In this study, the band observed at 1272 cm^{-1} in IR spectrum has been assigned to C–N stretching vibration of 4FA. The in-plane and out-of-plane bending C–N vibrations have also been identified and presented in TABLE 2 for the title compound. These assignments are also supported by the TED values.

NH_2 Group vibrations

The frequencies of amino group appear around 3500 cm^{-1}-3300 cm^{-1} for NH_2 stretching, 1700 cm^{-1}-1600 cm^{-1} for scissoring and 1150 cm^{-1}-900 cm^{-1} for rocking deformation [18]. In the present study, the asymmetric stretching modes of NH_2 group in 4FA are assigned at 3659 cm^{-1} in IR and 3506 cm^{-1} in Raman spectra. The symmetric stretching modes of NH_2 group are found at 3438 cm^{-1} and 3424 cm^{-1} in IR and Raman spectra, respectively. The band appeared at 1624 cm^{-1} in IR has been assigned to scissoring modes of NH_2 group for 4FA. The Rocking, wagging and twisting vibrational modes of NH_2 for the title compound are also presented in TABLE 2. The values computed theoretically, by B3LYP method, for NH_2 vibrational modes are in very good agreement with experimental data.

SERS spectra

Comparisons of the SERS spectra of the sample at different concentrations, with normal Raman spectra are shown in FIG. 5-9. It can be seen that main enhancement of lines is observed only in the region below 1000 cm^{-1}. There is moderate enhancement in the region between 1000 cm^{-1} and 2000 cm^{-1}. The enhancement is not very clear after 3000 cm^{-1}. Significant differences in relative intensities from SERS spectra are expected from the normal Raman spectrum, due to the specific surface selection rules [19].

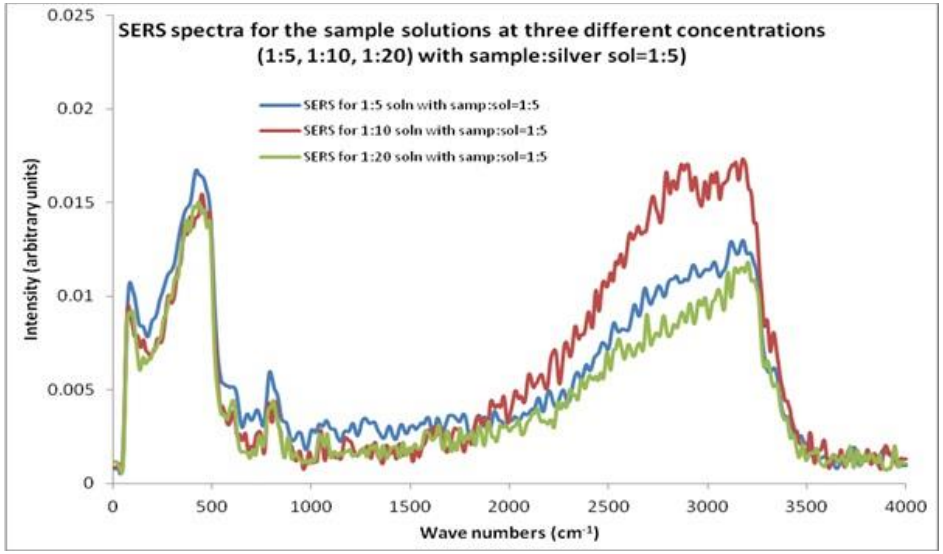

FIG. 5. **SERS spectra of the sample at three different concentrations (S1, S2, S3) with sample: sol ratio 1:5.**

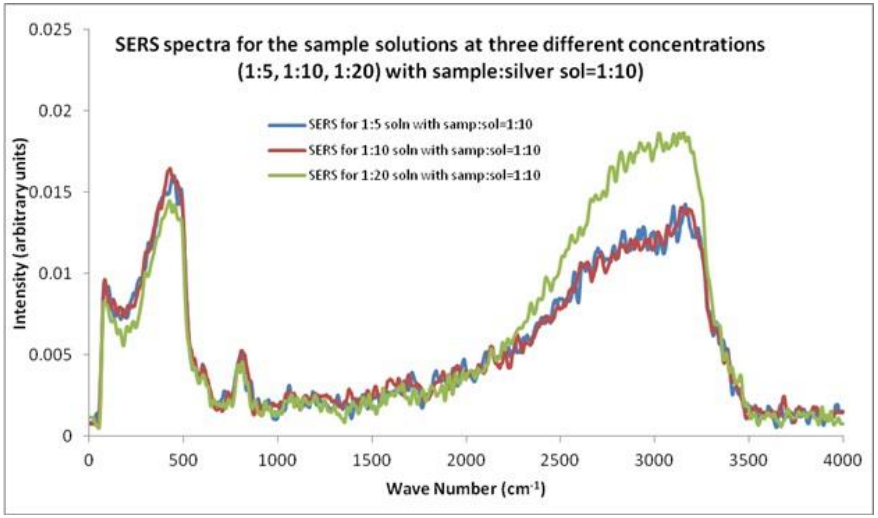

FIG. 6. **SERS spectra of the sample at three different concentrations (S1, S2, S3) with sample:sol ratio 1:10.**

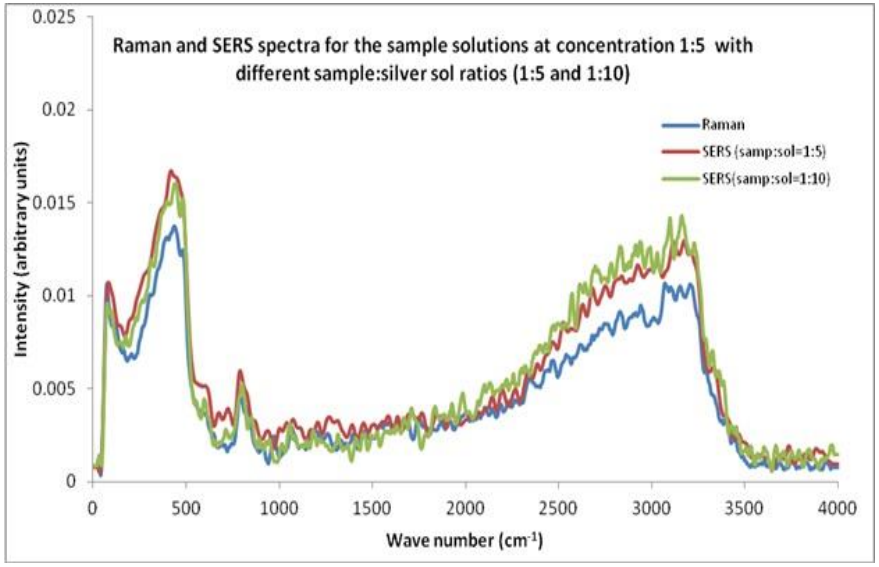

FIG. 7. **Comparison of Raman spectrum and SERS for sample S1.**

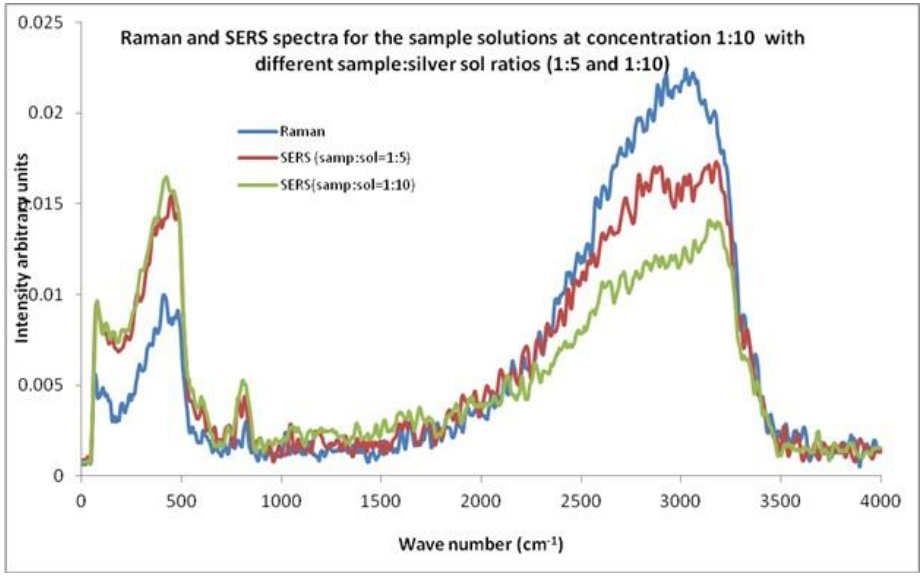

FIG. 8. **Comparison of Raman spectrum and SERS for sample S2.**

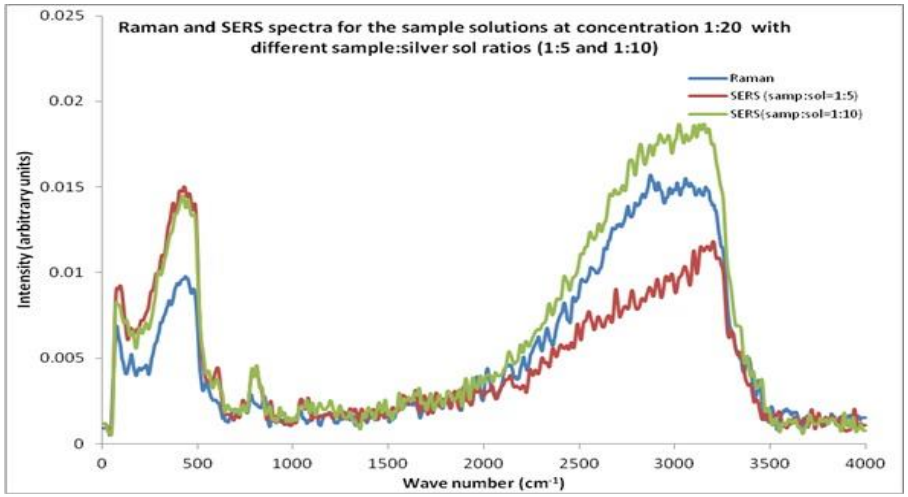

FIG. 9. **Comparison of Raman spectrum and SERS for sample S3.**

The surface selection rule suggests that for a molecule adsorbed flat on the silver surface, compared to the in-plane vibrational modes, the out of plane vibrational modes will be more enhanced and when it is adsorbed perpendicular to the surface the in-plane vibrational modes will be more enhanced than out of plane vibrational

modes [19,20]. It is further seemed that vibrations involving atoms that are close to the silver surface will be enhanced. In the normal Raman spectra of the three solutions a variation in intensity is observed. As expected, the intensity of Raman lines for the sample with higher concentration (blue line) is maximum, in the region upto 1600 cm^{-1}. But in 2000 to 3500 regions, the lowest concentration sample shows very high intensity, which can be due to excess of water.

In the region up to 600 cm^{-1}, there is considerable enhancement for almost all lines. But there is no considerable dependence of the enhancement on the concentration of the solution, as well as sample-sol ratio. However, there is a slight increase in the enhancement for the sample-sol ratio 1:5 and for the solution concentration 1:10. Even though there is considerable difference in the intensities of the lines in the region 2000 cm^{-1} to 3500 cm^{-1}, this cannot be fully attributed to the enhancement due to the metal surface, since the difference in water content also may contribute to this. It could be a combined effect of both.

First hyperpolarizability

The quantum chemistry based prediction of non-linear optical (NLO) properties of a molecule has an essential role in the design of materials in modern communication technology, signal processing and optical interconnections [21,22]. Such studies of organic molecules are more important because of their larger NLO susceptibilities arising from π-electron cloud movement from donor to acceptor, high laser damage thresholds, fast NLO response times and low dielectric constants. TABLE 3 shows the components of dipole moment, polarizability and the first hyperpolarizability of 4FA. The following equations [22] are used to calculate the average linear polarizability $\bar{\alpha}$, the total static dipole moment μ, the first hyperpolarizability β and the anisotropy of the polarizability Δα:

$$\bar{\alpha} = \frac{1}{3}(\alpha_{xx} + \alpha_{yy} + \alpha_{zz})$$

$$\Delta\alpha = \frac{1}{\sqrt{2}}\left[[(\alpha_{xx} - \alpha_{yy})^2 + (\alpha_{yy} - \alpha_{zz})^2 + (\alpha_{zz} - \alpha_{xx})^2 + 6\alpha_{xx}^2]\right]1/2$$

$$\mu = (\mu_x^2 + \mu_y^2 + \mu_z^2)^{1/2}$$

$$\beta = [(\beta_{xxx} + \beta_{xyy} + \beta_{xzz})^2 + (\beta_{yyy} + \beta_{xxy} + \beta_{yzz})^2 + (\beta_{zzz} + \beta_{xxz} + \beta_{yyz})^2]^{1/2}$$

The values calculated using the DFT-B3LYP/6-31+G (d, p) method are as follows:

Total static dipole moment μ=3.166 Debye

The average linear polarizability $\bar{\alpha}$ =11.482 $Å^3$

The anisotropy of the polarizability Δα=27.083 $Å^3$

The first hyperpolarizability β=0.798×10^{-30} $e.s.u.^{-1}$

The values of obtained by Sun et al. [23] with the B3LYP method for urea are:

μ=1.373 Debye,

$\overline{\alpha}$ =3.831 Å^3

And β=0.3729×10^{-30} e.s.u.$^{-1}$.

The first hyperpolarizability of 4FA molecule is 2 times greater than that of urea. According to these results, the title compound may be a potential candidate for the development of NLO materials.

TABLE 3. **Calculated dipole moment *μ* (Debye), polarizability *(α)* and the first hyperpolarizability *(β)* components (a.u.) for 4-fluoroaniline.**

Components	Values	Components	Values
μ_x	-3.0011	β_{xxx}	121.3888747
μ_y	-0.0005	β_{xxy}	0.0001906
μ_z	1.0085	β_{xyy}	-10.0299357
-	-	β_{yyy}	0.0038738
α_{xx}	101.7321162	β_{xxz}	7.0992237
α_{xy}	0.0000979	β_{xyz}	0.0225299
α_{yy}	84.6695337	β_{yyz}	7.2113197
α_{xz}	0.1856079	β_{xzz}	-25.6726973
α_{yz}	-0.0005829	β_{yzz}	-0.0065616
α_{zz}	46.2713182	β_{zzz}	20.2200354

HOMO, LUMO analysis

The frontier molecular orbitals (FMOs), i.e., highest occupied molecular orbitals (HOMOs) and the lowest unoccupied molecular orbitals (LUMOs), play an important role in the electric and optical properties, UV-Vis absorption as well as chemical reactions [24]. The energies of the highest and the second highest occupied MO's (HOMO and HOMO-1), the lowest and the second lowest unoccupied MO's (LUMO and LUMO+1) were calculated using B3LYP/6- 311++G (d, p). These are illustrated in FIG. 10. This indicates that4FA has 29 occupied MOs. The HOMO-LUMO energy gap for 4FA is found to be 5.1391 eV.

The LUMO: of π nature, (i.e. benzene ring) is delocalized over the whole C-C bond. By contrast, the HOMO is located over NH_2 group and fluorine atom; consequently the HOMO → LUMO transition implies an electron density transfer to C-C bond of the benzene ring from NH_2 group and fluorine atom. Moreover, these orbitals are found to overlap significantly in their position of the benzene ring for 4FA. The HOMO represents the ability to donate an electron and LUMO represents the ability to obtain an electron (electron acceptor). A decrease in HOMO-LUMO energy gap facilitates intra molecular charge transfer. This makes the material NLO active.

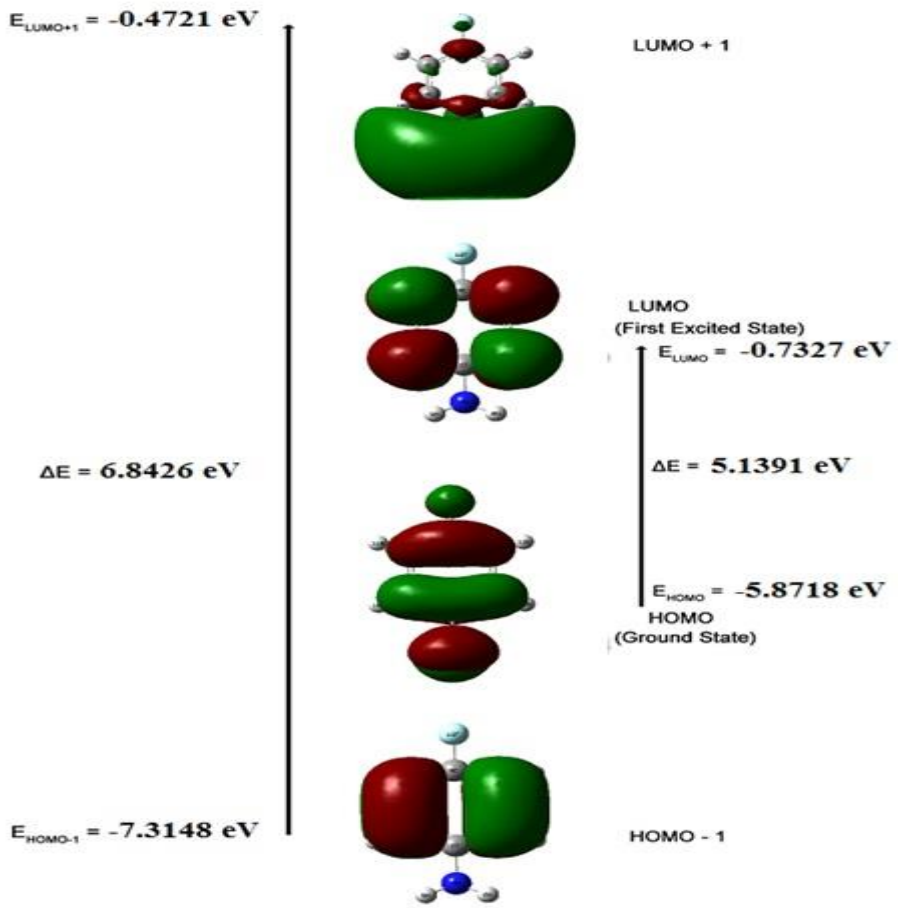

FIG. 10. **The atomic orbital HOMO and LUMO compositions of the frontier molecular orbital for 4-fluoroaniline.**

Mulliken population analysis

The calculation of Mulliken atomic charge [25] is important in the application of quantum chemical analysis to molecular systems due to the change in dipole moment, polarizability, electronic structure and much more properties of molecular systems. The total atomic charges of 4FA obtained by B3LYP method with 6-31+G (d, p) and 6-311++G (d, p) basis sets are listed in TABLE 4. The charge distribution on the molecule has an important influence on the vibrational spectra.

TABLE 4. **The charge distribution calculated by the Mulliken method.**

Atoms	Atomic charges (Mulliken)	
	B3LYP/6-31+G (d, p)	**B3LYP/6-311++G (d, p)**
C1	-0.086279	-0.590967
C2	0.013463	0.157407
C3	0.006318	0.066420
C4	-0.050909	-0.538783
C5	0.006254	0.066423
C6	0.013598	0.157446
N7	-0.595652	-0.301430
H8	0.286238	0.231949
H9	0.286231	0.231949
H10	0.114040	0.164176
H11	0.139411	0.190105
F12	-0.361007	-0.188972
H13	0.139411	0.190105
H14	0.114027	0.164173

The graphical representation of the results has been done in FIG. 11 and it gives us information about the charge shifts relative to 4FA. More charge density was found at C1, C4, N7 and F12 than that of other ring carbon atoms. The high positive charge at C2, C3, C5 and C6 is due to the effect of electron releasing NH_2 group and fluorine atom attached in the ring. The electron donating character of the NH_2 group in the title compound is demonstrated by a decrease in electron density on C1 atom. From the result it is clear that the substitution of NH_2 and fluorine atom in the aromatic ring leads to a redistribution of electron density.

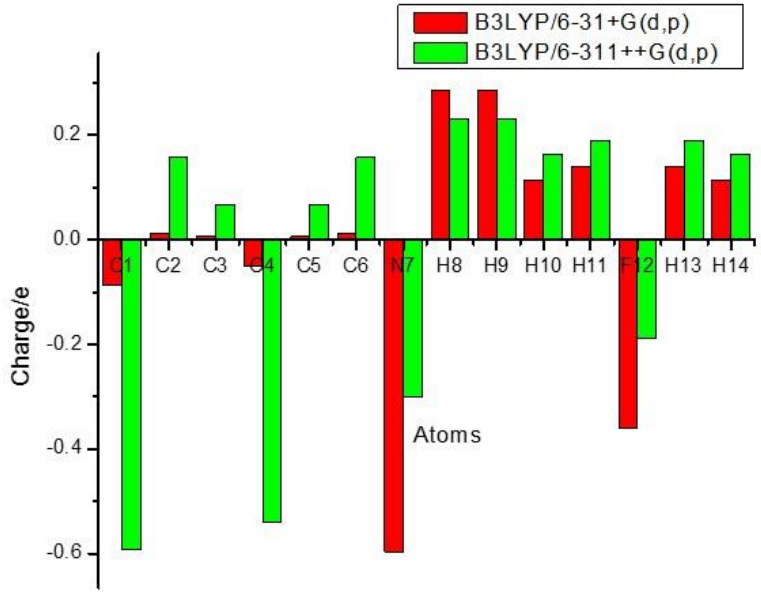

FIG. 11. **Mulliken's plot for 4-fluoroaniline.**

Electrostatic potential and molecular electrostatic potential total electron density

The electrostatic potential is used primarily for predicting sites and relative reactivities towards electrophilic attack and in studies of biological recognition and hydrogen bonding interactions [26,27]. The MEP at the B3LYP/6-31+G (d, p) optimized geometry was calculated, for predicting reactive sites for electrophilic and nucleophilic attack for the investigated molecule.

FIG. 12 shows the electron density (ED), electrostatic potential (ESP) and the molecular electrostatic potential (MEP) map figures for 4FA. The ED plots for the title molecule show a uniform distribution. However, the ESP figures show that the negative potential is localized more over the NH_2 group and fluorine atom and is reflected as a yellowish blob, the positive ESP is localized on the rest of the molecule. This result is expected, because ESP correlates with electro negativity and partial charges. The different values of the electrostatic potential at the surface are represented by different colours. Potential increases in the order red<orange<yellow<green<blue. In the FIG. 12, the positive (blue) regions to nucleophilic reactivity and the negative (red and yellow) regions of the MEP are related to electrophilic reactivity. As can be seen from the figure and the computed results, the MEP map shows that the negative potential sites are in fluorine atom and the positive region is over the hydrogen atoms of NH_2 group. From these results, the H atoms of NH_2 group indicate the strongest attraction and fluorine atom indicates the strongest repulsion. These sites give information about the region from where the compound can have intermolecular interactions. Thus, it would be predicted that the 4FA molecule will be the most reactive site for both electrophilic and nucleophilic attack.

Other molecular properties

Normally, the thermodynamical analysis on aromatic compound provides the necessary information regarding the chemical reactivity. TABLE 5 gives the standard statistical thermodynamic functions: heat capacity, zero point energy, entropy of 4FA, on the basis of vibrational analysis at B3LYP method. There is only a marginal difference in the values calculated by both the methods. The variation in the ZPVE seems to be significant. The molecular charge distribution is reflected by the dipole moment and is given as a vector in three dimensions. Therefore, it can be used as descriptor to depict the charge movement across the molecule.

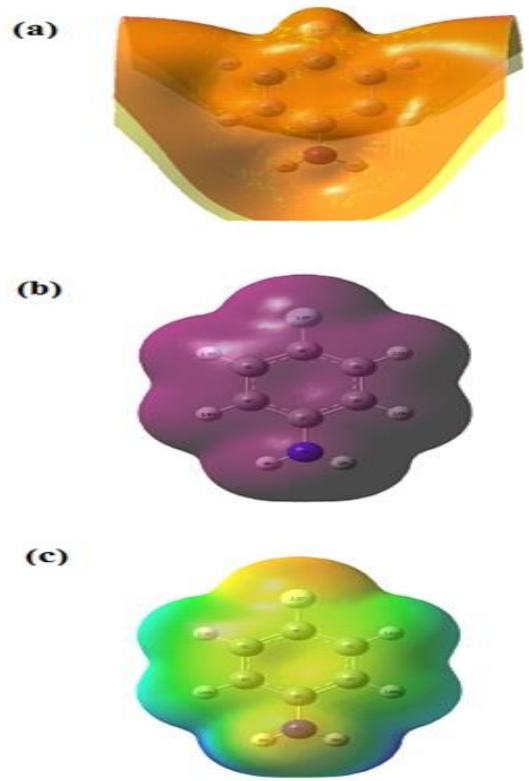

FIG. 12. **(a) Electrostatic potential (ESP) (b) Electron density (ED) and (c) The molecular electrostatic potential (MEP) map for 4-fluoroaniline.**

TABLE 5. **Thermodynamic properties of 4-fluoroaniline.**

Parameters	Method/Basis set	
	B3LYP/6-31+G (d, p)	**B3LYP/6-311++G (d, p)**
Optimized global minimum energy (Hartrees)	-386.86972381	-386.95473148
Total energy (thermal), E_{total} (kcal mol^{-1})	72.375	72.130
Heat capacity, C_v (cal mol^{-1} k^{-1})	26.377	26.413
Entropy, S (cal mol^{-1} k^{-1})	-	-
Total	80.415	80.430
Translational	40.030	40.030
Rotational	27.951	27.937
Vibrational	12.434	12.462
Vibrational energy, E_{vib} (kcal mol^{-1})	70.597	70.352
Zero point vibrational energy, (kcal mol^{-1})	68.17493	67.92611
Rotational constants (GHz)	-	-
A	5.57988	5.61161
B	1.43787	1.44350
C	1.14436	1.14928
Dipole moment (Debye)	-	-
μ_x	-3.0011	2.9829
μ_y	-0.0005	0.0000
μ_z	1.0085	0.9871
μ_{total}	3.1660	3.1420

Direction of the dipole moment vector in a molecule depends on the centers of positive and negative charges. The total dipole moment of 4FA determined by the B3LYP method using 6-31+G (d, p) and 6-311++G (d, p) basis sets are 3.166 and 3.142 Debye, respectively. The total energy and the change in the total entropy of the compound at room temperature are also presented. All the thermodynamic data are helpful for the further study on the 4FA. They can be used to compute the other thermodynamic energies and estimate directions of chemical reactions.

Conclusion

The molecular structural parameters and fundamental vibrational frequencies of 4-fluoroaniline have been obtained from DFT/B3LYP calculation. The effect of halogen substituent on vibrational frequencies is analysed in detail. In the present, most of the fundamentals are believed to be assigned, unambiguously. The SERS spectra show enhancement in most of regions of the spectra. But concentration dependence of the enhancement is not very clear.

The frequency assignments are strongly supported by the TED calculation about the normal modes of vibratio. The calculated first order hyperpolarizability was found to be 0.798×10^{-30} esu, which is 2 times greater than reported in literature for urea. The HOMO and LUMO energy gap shows that the charge transfer occurs within the molecule, which is responsible for the bioactive property of the molecule. The MEP map predicts the reactive sites for electrophilic and nucleophilic attack the molecule and the results are discussed. Furthermore, the thermodynamic and Mulliken charge analysis of the compound have been calculated in order to get insight into the compound.

REFERENCES

1. Diaz FR, Sanchez CO, Del Valle MA, et al. Synthesis, characterization and electrical properties of poly (2, 5-, 2, 3- and 3, 5-dichloroaniline) s: Part II. Copolymers with aniline. Synth Met. 2001;118:25-31.
2. Dong Y, Mu S. Photoelectrochemical behaviour of polyaniline affected by potentials and pH of solutions. Electrochem Acta. 1991;36:2015-8.
3. Evgen'ev MI, Evgen'eva II, Garmonov SY, et al. Sorption-Chromatographic Determination of Aniline, 4-Chloroaniline and 2, 5-Dichloroaniline in Air. J Analyt Chem. 2003;58:542-7.
4. Wojciechowski PM, Michalska D. Theoretical Raman and infrared spectra and vibrational assignment for para-halogenoanilines: DFT study. Spectrochim Acta. 2007;68:948-55.
5. Kavitha E, Sundaraganesan N, Sebastian S. Molecular structure, vibrational spectroscopic and HOMO, LUMO studies of 4-nitroaniline by density functional method. Ind J Pure Appl Phys. 2010;48:20-30.
6. Arjunan V, Rani T, Mohan S. Spectroscopic and quantum chemical electronic structure investigations of 2-(trifluoromethyl) aniline and 3-(trifluoromethyl) aniline. J Mol Struct. 2011;994:179-93.
7. Femina Jasmine G, Amalanathan M, Dawn Dharma Roy S. Molecular structure and charge transfer contributions to nonlinear optical property of 2-Methyl-4-nitroaniline: A DFT study. J Mol Struct. 2016;1112:63-70.
8. Revathi B, Balachandran V, Raja B, et al. Potentially useful to NLO materials: 4-Chloro-3-(trifluoromethyl) aniline, 4-bromo-3-(trifluoromethyl) aniline and 4-fluoro-3-(trifluoromethyl) aniline are combined experimental and theoretical vibrational analysis. J Mol Struct. 2017;1141:81-92.
9. Creighton JA, Blatchford CG, Albrecht MG. Plasma resonance enhancement of Raman scattering by pyridine adsorbed on silver or gold sol particles of size comparable to the excitation wavelength. J Chem Soc Farad Trans. 1979;75:790-8.
10. Frisch MJ, Trucks GW, Schlegel HB, et al. Gaussian09, Revision A.02, Gaussian Inc., Wallingford CT, 2009.

11. Sundius T. 'Scaling of ab initio force fields by MOLVIB. Vib Spectrosc. 2002;29:89-95.
12. Molvib V. 7.0: Calculation of Harmonic Force Fields and Vibrational Modes of Molecules, QCPE Program No. 202;807.
13. Colapietro M, Domenicano A, Marciante C, et al. Structural studies of benzene derivatives. IX. The structures of p-fluoroaniline and p-cyanoaniline hydrochlorides. Acta Cryst. 1981;B37:387-94.
14. Arivazhagan M, Jeyavijayan S, Geethapriya J. Conformational stability, vibrational spectra, molecular structure, NBO and HOMO–LUMO analysis of 5-nitro-2-furaldehyde oxime based on DFT calculations. Spectrochim Acta. 2013;104A:14-25.
15. Jeyavijayan S. Spectroscopic (FTIR, FT-Raman), molecular electrostatic potential, NBO and HOMO–LUMO analysis of P-bromobenzene sulfonyl chloride based on DFT calculations. Spectrochim Acta. 2015;136A:890-9.
16. Gunasekaran S, Seshadri S, Muthu S, Vibrational spectra and normal coordinate analysis of flucytosine. Indian J Pure Appl Phys. 2006;4:581-6.
17. Arivazhagan M, Jeyavijayan S. Vibrational spectroscopic, first-order hyperpolarizability and HOMO, LUMO studies of 1, 2-dichloro-4-nitrobenzene based on Hartree-Fock and DFT calculations. Spectrochim Acta. 2011;79A:376-83.
18. Socrates G. Infrared and Raman Characteristic Group Frequencies-TABLES at Charts. 3rd ed. Wiley; New York. 2001.
19. Gao X, Davies JP, Weaver MJ. Test of surface selection rules for surface-enhanced Raman scattering: The orientation of adsorbed benzene and monosubstituted benzenes on gold. J Phys Chem. 1990;94:6858-64.
20. Cross AD. Introduction to Practical Infrared Spectroscopy. London; Butterworths Scientific Publications. 1960.
21. Geskin VM, Lambert C, Bredas JL. Origin of high second- and third-order nonlinear optical response in ammonio/borato diphenylpolyene zwitterions: The remarkable role of polarized aromatic groups. J Am Chem Soc. 2003;125:15651-8.
22. Sajan D, Hubert Joe I, Jayakumar VS, et al. Structural and electronic contributions to hyperpolarizability in methyl p-hydroxy benzoate. J Mol Struct. 2006;785:43-53.
23. Sun YX, Hao QL, Wei WX, et al. Experimental and density functional studies on 4-(3, 4-dihydroxybenzylideneamino) antipyrine and 4-(2, 3, 4-trihydroxybenzylideneamino) antipyrine. J Mol Struct (Theochem.) 2009;904:74-82.
24. Fleming I. Frontier Orbitals and Organic Chemical Reactions, Wiley; London. 1976.
25. Rastogi VK, Palafox MA, Mittal L, et al. FTIR and FT-Raman spectra and density functional computations of the vibrational spectra, molecular geometry and atomic charges of the biomolecule: 5-bromouracil. J Raman Spectrosc. 2007;38:1227-41.
26. Murray JS, Sen K. Molecular Electrostatic Potentials, Concepts and Applications, Elsevier; Amsterdam. 1996;pp:7-624.
27. Scrocco E, Tomasi J. Electronic molecular structure, reactivity and intermolecular forces: An euristic interpretation by means of electrostatic molecular potentials. Adv Quantum Chem. 1978;11:115-93.